# Structure and dynamics of bulk liquid Ga and the liquid-vapor interface: An *ab initio* study

Luis E. González and David J. González
*Departamento de Física Teórica, Universidad de Valladolid, 47011 Valladolid, Spain*
(Received 1 June 2007; revised manuscript received 17 January 2008; published 20 February 2008)

The static and dynamic structure of bulk liquid gallium is studied by using the orbital-free *ab initio* molecular dynamics method. Three thermodynamic states along the coexistence line are considered, namely, $T=373$, 523, and 959 K for which x-ray and/or neutron scattering data are available. The calculated static structure shows good agreement with the available experimental data. The dynamical structure reveals collective density excitations with an associated dispersion relation, which closely follows recent experimental data. Results have also been obtained for several transport coefficients. The overall picture is that the dynamic properties have many characteristics of the simple liquid metals. Additional simulations have also been performed on the structure of the free liquid surface associated with those thermodynamic states. We analyze its oscillatory ionic and valence electronic longitudinal density profiles, and comparison is made with the corresponding experimental data.

DOI: 10.1103/PhysRevB.77.064202 PACS number(s): 61.20.Ja, 61.20.Lc, 61.25.Mv, 71.15.Pd

## I. INTRODUCTION

The *ab initio* molecular dynamics (AIMD) methods based on the density functional theory[1] (DFT) have become a usual technique for the study of liquid systems. Starting with a collection of atoms at given nuclear positions, the DFT enables us to compute the ground state electronic energy and, via the Hellmann-Feynman theorem, it also yields the forces on the nuclei. It enables us to perform molecular dynamics (MD) simulations in which the nuclear positions evolve according to classical mechanics, whereas the electronic subsystem follows adiabatically. Most AIMD methods are based on the Kohn-Sham (KS) orbital representation of the DFT (KS-AIMD methods), which poses heavy computational demands and therefore somehow limits the size of the systems under study as well as the simulation times. However, some of those constraints can be brushed away by the so-called orbital-free *ab initio* molecular dynamics (OF-AIMD) method, which by disposing of the electronic orbitals of the KS formulation provides a simulation method, where the number of variables describing the electronic state is greatly reduced, enabling the study of larger samples (thousands of particles) and for longer simulation times (tens of picoseconds).

This paper reports an *ab initio* molecular dynamics simulation on several static and dynamic properties of liquid gallium (l-Ga) at three thermodynamic states along the coexistence line. Gallium is an interesting material with peculiar structural and electronic properties. Besides a very low melting point (303 K), it exhibits a wide variety of morphological crystalline structures, which include both covalent and metallic bondings. At ambient pressure,[2,3] the stable crystalline structure is the orthorhombic $\alpha$-Ga with seven nearest neighbors and combines metallic bonding with strong $Ga_2$ covalent bonds. Upon application of pressure, it transforms to a metallic phase, Ga II, with a complicated structure comprising 104 atoms in the unit cell. At melting, l-Ga has a higher density than the stable solid $\alpha$-Ga, it has 10–11 nearest neighbors, and its static structure factor $S(q)$ exhibits a main peak with a shoulder characteristic of nonclosed packed structures.

Most theoretical studies on l-Ga have focused on its static structural properties and the vast majority were performed by classical MD simulations where the liquid system was characterized by effective interatomic potentials constructed by means of some approximate theoretical model.[4–6] To our knowledge, only two KS-AIMD-type calculations[7,8] have been performed; however, the serious computational constrains inherent to this method have imposed some limitations on the calculated properties.

Gong *et al.*[7] performed the first KS-AIMD calculation of the electronic and static properties of bulk l-Ga at $T=1000$ K; the calculation used 64 particles, a separable pseudopotential, and the local density approximation (LDA) for the electronic exchange and correlation energies. Subsequently, another KS-AIMD calculation for l-Ga at $T=702$ and 982 K was carried out by Holender *et al.*[8] by using 64 particles, a norm conserving nonlocal pseudopotential, and the LDA. Besides the electronic and static properties, this calculation also yielded some results for a collective property; namely, the dynamical structure factor.

The *ab initio* studies have provided accurate descriptions of the local liquid structure, as well as valuable insights into the properties of the valence electronic charge densities. Indeed, it was found[7] that covalent and metallic characters coexist in l-Ga, with the covalent aspect evidenced by the existence of some very short lived $Ga_2$ covalent molecules with bonds similar to those of $\alpha$-Ga. On the other hand, the calculated dynamic structure factors[8] revealed the existence of density fluctuations up to a wave vector of 1.8 $Å^{-1}$. However, these KS-AIMD studies could only be afforded to be performed at high temperatures because of the high mobility required for a fast thermalization of the simulated sample. Consequently, the region around the melting point, for which a wealth of experimental data is available, was left aside. Furthermore, there are other dynamical properties of l-Ga, not yet evaluated, that will constitute a substantive part of the present study; which, to our knowledge, is the first *ab initio* study on the dynamical properties of bulk l-Ga near melting.

On the experimental front, the static structure factor of l-Ga has already been measured by both neutron scattering[9] (NS) and x-ray[10] diffraction. As for the dynamical structure, it has also been investigated by both inelastic neutron scattering[11–13] (INS) and inelastic x-ray scattering (IXS).[14–16] The INS measurements of Bermejo *et al.*[11] for l-Ga near

 

melting found no inelastic peaks in the low-$q$ region, where—according to the hydrodynamic theory—they should have been expected. This absence was rationalized in terms of an overdamping effect induced by the very high value of the longitudinal viscosity. Subsequently, another INS experiment[12] for l-Ga at a higher temperature ($T$=973 K) found, in that low-$q$ region, two (low and high frequencies) branches of collective excitations which were linked to acoustic and optic modes, respectively. This discrepancy between the low and high temperature experimental results was attributed to a sharp viscosity drop with increasing temperature.

More recently, an IXS experiment by Scopigno *et al.*,[14] for l-Ga near melting, has unambiguously unveiled the existence of collective excitations in the same low-$q$ region where the previous INS measurements[11] had suggested an overdamped regime. Indeed, these measurements found that the collective density excitations in l-Ga exhibited a pattern very similar to that of the liquid simple metals[17,18] near melting. These findings have recently been corroborated by additional IXS[16] and INS[13] measurements. Specifically, those of Hosokawa *et al.*[16] were performed for l-Ga at $T$=373 K. They investigated the wave vector regions $0.03 \leq q \leq 2.8$ Å$^{-1}$, obtaining several dynamical features already observed in the liquid alkali metals, such as the existence of collective excitations up to $q$ values around $0.5q_p$ [where $q_p$ is the main peak's position of $S(q)$] which, moreover, exhibit a positive dispersion of $\approx 15\%$ in the $q$-dependent adiabatic sound velocity with respect to the hydrodynamic value. On the other hand, the INS data of Bove *et al.*[13] were obtained for l-Ga at $T$=320 and 970 K and spanned a region of $0.25 \leq q \leq 1$ Å$^{-1}$. Besides corroborating the previous IXS findings for the collective dynamics (i.e., the occurrence of propagating density fluctuations), their INS data have provided new insights into the single particle dynamics. Specifically, it was found that, within the explored $q$ range, two different time scales are needed to adequately account for the self-dynamics; the slower one was associated with the usual diffusion process, whereas the faster one described the residence time of an atom within the cage of its nearest neighbors. Consequently, it was shown that a two-Lorentzian function model was the more adequate to describe the experimental self-dynamical structure.

The free liquid surface of l-Ga has also attracted some interest, and x-ray reflectivity (XR) measurements have been performed on l-Ga over a range of temperatures from 295 to 443 K.[19–21] The reflectivity was measured up to wave vector transfers of $q_z$=3.0 Å$^{-1}$, showing a marked peak at around $q_z$=2.4 Å$^{-1}$. This is indicative of an oscillatory (longitudinal) ionic density profile (DP) along the normal to the liquid surface, which extends for several atomic diameters into the bulk liquid. Moreover, it was found that the amplitude of the peak decreases drastically upon heating along the previous temperature range. This has been linked to the temperature dependence of capillary-wave induced surface roughness. More recently, x-ray diffuse scattering measurements by Lin *et al.*[22] have shown the wavelength dependent surface tension on l-Ga at 308 K. On the theoretical side, we single out the studies of Zhao *et al.*[23,24] on the free liquid surface of l-Ga near melting, which were performed by self-consistent Monte Carlo (MC) simulations based on density dependent pair potentials derived from pseudopotentials. They obtained an oscillating longitudinal ionic DP lasting for around four atomic diameters into the bulk liquid, which is in agreement with experiment. Furthermore, the calculated longitudinal electronic valence DP also exhibited weaker oscillations that were clearly in the opposite phase of the ionic ones.

The layout of this paper is as follows. In Sec. II, we provide a brief review of the OF-AIMD method, with special emphasis on the electronic kinetic energy functional and the local pseudopotential used to characterize the ion-electron interaction. Section III presents the results obtained for several static and dynamic properties of bulk l-Ga at three thermodynamic states ranging from near melting up to the high temperature state considered in the aforementioned KS-AIMD studies.[7,8] The structure of the liquid-vapor interface is calculated in Sec. IV, where several structural magnitudes are evaluated and discussed. In both sections, a comparison is made with the available experimental data. Finally, some conclusions are drawn and possible ideas for further improvements are suggested.

## II. THEORY

A simple liquid metal is treated as a disordered array of $N$ bare ions with valence $Z$, enclosed in a volume $V$, and interacting with $N_e=NZ$ valence electrons through an electron-ion potential $v(r)$. The total potential energy of the system can be written, within the Born-Oppenheimer approximation, as the sum of the direct ion-ion Coulombic interaction energy and the ground state energy of the electronic system under the external potential created by the ions $V_{\text{ext}}(\mathbf{r},\{\mathbf{R}_I\}) = \sum_{i=1}^{N} v(|\mathbf{r}-\mathbf{R}_i|)$,

$$E(\{\mathbf{R}_I\}) = \sum_{i<j} \frac{Z^2}{|\mathbf{R}_i - \mathbf{R}_j|} + E_g[\rho_g(\mathbf{r}), V_{\text{ext}}(\mathbf{r},\{\mathbf{R}_I\})], \quad (1)$$

where $\rho_g(\mathbf{r})$ is the ground state electronic density and $\mathbf{R}_I$ are the ionic positions. According to DFT, the ground state electronic density $\rho_g(\mathbf{r})$ can be obtained by minimizing the energy functional $E[\rho]$, which can be written as

$$E[\rho(\mathbf{r})] = T_s[\rho] + E_H[\rho] + E_{\text{xc}}[\rho] + E_{\text{ext}}[\rho], \quad (2)$$

where the terms represent, respectively, the electronic kinetic energy $T_s[\rho]$ of a noninteracting system of density $\rho(\mathbf{r})$, the classical electrostatic energy (Hartree term)

$$E_H[\rho] = \frac{1}{2}\int\int d\mathbf{r}d\mathbf{s}\frac{\rho(\mathbf{r})\rho(\mathbf{s})}{|\mathbf{r}-\mathbf{s}|}, \quad (3)$$

the exchange-correlation energy $E_{\text{xc}}[\rho]$, for which we have used the generalized gradient approximation,[25] and finally the electron-ion interaction energy

$$E_{\text{ext}}[\rho] = \int d\mathbf{r}\rho(\mathbf{r})V_{\text{ext}}(\mathbf{r}), \quad (4)$$

where the electron-ion potential has been characterized by a local ionic pseudopotential constructed within DFT.[18]

In the KS-AIMD method,[1] $T_s[\rho]$ is exactly evaluated by using single particle orbitals, which requires a huge compu-

tational effort. This is ameliorated in the OF-AIMD approach[1,18,26] by using an explicit albeit approximate functional of the density for $T_s[\rho]$. The proposed functionals consist of the von Weizsäcker term,

$$T_W[\rho(\mathbf{r})] = \frac{1}{8}\int d\mathbf{r}|\nabla\rho(\mathbf{r})|^2/\rho(\mathbf{r}), \quad (5)$$

plus further terms chosen in order to correctly reproduce some exactly known limits. Here, we have used an average density model,[18] where $T_s = T_W + T_\alpha$,

$$T_\alpha = \frac{3}{10}\int d\mathbf{r}\rho(\mathbf{r})^{5/3-2\alpha}\tilde{k}(\mathbf{r})^2,$$

$$\tilde{k}(\mathbf{r}) = (2k_F^0)^3\int d\mathbf{s}k(\mathbf{s})w_\alpha(2k_F^0|\mathbf{r}-\mathbf{s}|), \quad (6)$$

$k(\mathbf{r}) = (3\pi^2)^{1/3}\rho(\mathbf{r})^\alpha$, $k_F^0$ is the Fermi wave vector for mean electron density $\rho_e = N_e/V$, and $w_\alpha(x)$ is a weight function chosen so that both the linear response theory and Thomas-Fermi limits are correctly recovered. Further details are given in Ref. 18.

Another key ingredient of the energy functional is the local ionic pseudopotential $v_{ps}(r)$ describing the ion-electron interaction. It has been constructed from first principles by fitting, within the same $T_s[\rho]$ functional, to the displaced electronic density induced by an ion embedded in a metallic medium as obtained in a KS-DFT calculation. Further details are given in Ref. 18 and we just note that the previous theoretical framework has already delivered an accurate description of several static and dynamic properties of bulk liquid Li, Mg, Al, Na-Cs, and Li-Na systems[18,27] as well as some liquid-vapor (LV) interfaces.[28]

## III. RESULTS: BULK PROPERTIES

OF-AIMD simulations were performed for bulk l-Ga at three thermodynamic states. We have considered 2000 ions in a cubic cell with periodic boundary conditions and whose size was appropriate for the corresponding experimental[29] bulk ionic number density; additional details are given in Table I. Given the ionic positions at time $t$, the electronic energy functional is minimized with respect to $\rho(\mathbf{r})$, represented by a single *effective orbital* $\psi(\mathbf{r})$, defined as $\rho(\mathbf{r}) = \psi(\mathbf{r})^2$. The orbital is expanded in plane waves which are truncated at some cutoff energy $E_{\text{cut}}$. The energy minimization with respect to the Fourier coefficients of the expansion is performed every ionic time step by using a quenching method, which results in the ground state electronic density and energy. The forces on the ions are obtained from the electronic ground state via the Hellman-Feynman theorem, and the ionic positions and velocities are updated by solving Newton's equations, with the Verlet leapfrog algorithm. In the simulations, the equilibration process lasted 15 ps and the calculation of properties was made averaging over 80 ps. For comparison, recall that the two forementioned KS-AIMD simulations lasted for 2.5 (Ref. 7) and 8.0 ps,[8] which underscores its limitations for addressing the dynamical properties.

TABLE I. Input data for the thermodynamic states of bulk l-Ga studied in this work, along with some simulation details. $L_0$ is the side of the simulation box, $\delta t$ is the ionic time step, and $E_{\text{cut}}$ is the cutoff energy.

| $T$ (K) | $\rho_i$ (Å$^{-3}$) | $L_0$ (Å) | $\delta t$ (ps) | $E_{\text{cut}}$ (Ry) |
|---|---|---|---|---|
| 373 | 0.0512 | 33.924 | 0.005 | 15.5 |
| 523 | 0.0505 | 34.086 | 0.005 | 15.5 |
| 959 | 0.0490 | 34.431 | 0.005 | 15.5 |

We have evaluated several liquid static properties (pair distribution function and static structure factor) and dynamic properties, both single-particle ones (velocity autocorrelation function and mean square displacement) and collective ones (intermediate scattering functions, dynamic structure factors, and longitudinal and transverse currents). The calculation of the time correlation functions (CFs) was performed by taking time origins every five time steps. Several CFs also have a dependence on the wave vectors $\mathbf{q}$ which, as our system is isotropic, depend on $q \equiv |\mathbf{q}|$ only.

### A. Static properties

Figure 1 depicts the calculated static structure factors $S(q)$ along with the x-ray diffraction data of Waseda[10] and the NS data of Bellissent-Funel *et al.*[9] The OF-AIMD based $S(q)$ at $T=373$ K exhibits a main peak at $q_p \approx 2.51$ Å$^{-1}$, along with the characteristic shoulder at $\approx 3.10$ Å$^{-1}$, and the second peak is at $\approx 4.87$ Å$^{-1}$. As for the experimental $S(q)$'s, we note that for $T=363$ K, the NS data of Bellissent-Funel *et al.*[9] show a main peak at $\approx 2.53$ Å$^{-1}$, with the shoulder at $\approx 3.0$ Å$^{-1}$, and the second peak at $\approx 4.87$ Å$^{-1}$. The OF-AIMD results for $T=373$ and 523 K overestimate the amplitude of the main peak, but the amplitude and phase of the subsequent oscillations are well reproduced. A good agreement with experiment is obtained for $S(q)$ at $T=959$ K; indeed, this accuracy is comparable to that achieved by the KS-AIMD results of Gong *et al.*[7] at $T=1000$ K and Holender *et al.*[8] at $T=982$ K. However, these latter ones display a spiky shape in the region around the first peak.

Extrapolation of $S(q)$ to $q \to 0$ allows the isothermal compressibility $\kappa_T$ to be estimated from the relation $S(q \to 0) = \rho k_B T \kappa_T$. A least-squares fit of $S(q) = s_0 + s_2 q^2$ to the calculated $S(q)$ for $q$ values up to 0.6 Å$^{-1}$ yields the result of $\kappa_{T,\text{OF-AIMD}} = 2.20 \pm 0.2$ for $T=373$ K (in $10^{-11}$ m$^2$ N w$^{-1}$ units), which is close to the experimental value at the same temperature,[29] namely, $\kappa_T = 2.05 \pm 0.10$. For the higher temperatures $T=523$ and 959 K, we have obtained $\kappa_{T,\text{OF-AIMD}} = 2.4 \pm 0.2$ and $2.6 \pm 0.3$, whereas their respective experimental data[29] are $\kappa_T = 2.10 \pm 0.1$ and $2.50 \pm 0.1$. Additionally, the KS-AIMD study of Holender *et al.*[8] yielded a value $\kappa_{T,\text{KS-AIMD}} = 2.4 \pm 0.3$ for $T=702$ K, whereas the experimental value was $\kappa_T = 2.2 \pm 0.1$.

The pair distribution function $g(r)$ is also directly evaluated during the simulations. Its main peak's position is usually identified with the average nearest neighbor distance,

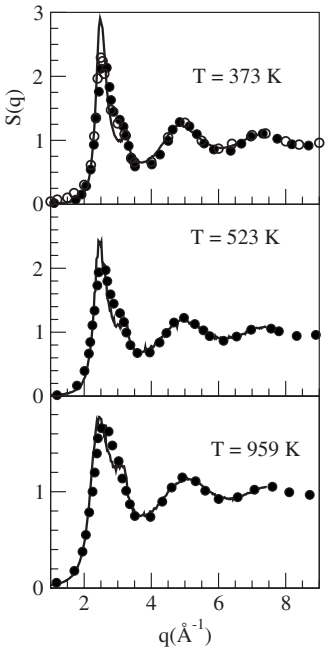


FIG. 1. Static structure factors of bulk l-Ga. Continuous line: OF-AIMD simulations at $T=373$, 523, and 959 K. Full circles: experimental NS data (Ref. 9) at $T=363$, 523, and 959 K. Open circles: experimental x-ray diffraction data (Ref. 10) at $T=323$ K.

which in the present OF-AIMD calculation stands at $\approx 2.80$ Å for $T=373$ K, and slightly reduces to $\approx 2.78$ Å for $T=523$ K and $\approx 2.73$ Å for $T=959$ K. Also, a similar trend is displayed by the experimental $g(r)$'s of Bellisent–Funel *et al.*[9] where the main peak's position decreases from $\approx 2.76$ Å for $T=326$ K to $\approx 2.70$ Å for $T=959$ K. This latter value was also obtained in the KS-AIMD calculation[8] of l-Ga at $T=982$ K. The number of nearest neighbors, also known as the coordination number (CN), is obtained by integrating the radial distribution function (RDF), $4\pi r^2 \rho_i g(r)$, up to a distance $r_m$ which is usually identified as the position of the first minimum in the RDF.[30,31] Our calculations give $r_m \approx 3.81$, 3.72, and 3.45 Å for $T=373$, 523, and 959 K, leading to CN $\approx 11.8$, 11.2, and 8.5 atoms, respectively. A similar calculation made by using the experimental $g(r)$ of Bellisent-Funel *et al.*[9] gave CN $\approx 10.5$ and 8.7 atoms for $T=326$ and 959 K, respectively. On the other hand, we note that the previous KS-AIMD studies of l-Ga at $T=1000$ and 982 K gave CN $\approx 8.9$ and 9.1, respectively.[7,8]

### B. Dynamic properties

#### 1. Collective dynamics

The intermediate scattering function $F(q,t)$ contains both spatial and temporal information on the collective dynamics of density fluctuations. It is defined as

$$F(q,t) = \frac{1}{N}\left\langle \left( \sum_{j=1}^{N} e^{-i\mathbf{q}\mathbf{R}_j(t+t_0)} \right) \left( \sum_{l=1}^{N} e^{i\mathbf{q}\mathbf{R}_l(t_0)} \right) \right\rangle. \qquad (7)$$

Its frequency spectrum is the dynamic structure factor $S(q,\omega)$, which can be directly measured by either INS or IXS experiments. For the three thermodynamic states, the calculated $F(q,t)$ exhibit a marked oscillatory behavior with the amplitude of the oscillations being stronger for the smaller $q$ values, and this is superposed on a very weak diffusive component. Indeed, this is a typical trend found for other simple liquid metals near melting by either computer simulations[18,32–34] or theoretical models,[35] and it gives rise to clearly defined inelastic peaks in the $S(q,\omega)$.

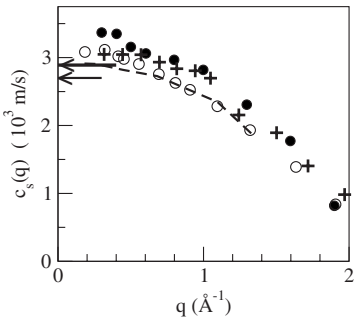


FIG. 2. $q$-dependent sound velocity $c_s(q)$ for liquid Ga. Open circles: OF-AIMD results. Full circles: experimental $c_s(q)$ at $T=373$ K from Hosokawa *et al.* (Ref. 16). Crosses: experimental $c_s(q)$ at $T=315$ K from Scopigno *et al.* (Ref. 14). Dashed line: OF-AIMD results for $T=959$ K. The arrows show the experimental adiabatic sound velocities of 2890 and 2700 m/s for $T=373$ and 959 K, respectively.

For all states, we have found that the side peaks in the corresponding $S(q,\omega)$ last up to $q \approx (3/5)q_p$. Moreover, from the positions of the side peaks $\omega_m(q)$, the dispersion relation of the density fluctuations is obtained and its slope at $q=0$ provides an estimate for the adiabatic sound velocity $c_s$. Thus, for $T=373$ K, we have obtained $c_s=2920\pm 150$ m/s, which compares well with the corresponding experimental data[29] of $c_s=2890\pm 50$ m/s. Hosokawa *et al.*[16] measured the $q$-dependent adiabatic sound velocity, defined as $c_s(q)=\omega_l(q)/q$, where $\omega_l(q)$ is the maximum frequency of the longitudinal current correlation function $J_l(q,\omega)=\omega^2 S(q,\omega)$. In the low-$q$ region, the experimental $c_s(q)$ data exhibit a *positive dispersion*, i.e., an increase with respect to the hydrodynamic adiabatic speed of sound, with a maximum located around 0.3 Å$^{-1}$ and whose magnitude amounts to $\approx 15\%$. This value is greater than the $\approx 7\%$ result obtained from the IXR data of Scopigno *et al.*[14] for a slightly lower temperature ($T=315$ K). Both sets of data are plotted in Fig. 2 where we have also included our calculated $c_s(q)$ values which predict a *positive dispersion* of $\approx 8\%$. Analogously, for the higher temperatures, $T=523$ and 959 K, the OF-AIMD calculation gives $c_s=2875$ and $2750\pm 150$ m/s, which are close to their respective experimental values[29] of $c_s=2840$ and $2700\pm 50$ m/s. Moreover, for $T=959$ K, the present calculations still predict a positive dispersion of $\approx 5\%$.

More recently, Scopigno *et al.*[15] performed another set of IXS measurements on $S(q,\omega)$ of liquid Ga at $T=315$ K, and for wave vectors up to $3q_p$. Their results showed that for $q \leq 2$ Å$^{-1}$, the associated $S(q,\omega)$ may be described in terms of three Lorentzian lines; whereas for greater $q$ values, it practically reduces to the central one, which stands for the quasi-

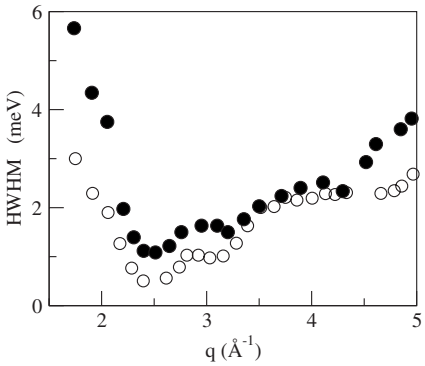


FIG. 3. HWHM of the dynamic structure factor for liquid Ga. Full circles: experimental data at $T=315$ K from Scopigno *et al.* (Ref. 15). Open circles: Present OF-AIMD results for $T=373$ K.

elastic extended heat mode. Figure 3 shows the experimental data for the half-width at half maximum (HWHM) of the quasielastic heat mode; it exhibits oscillations clearly connected with those of the $S(q)$. Most noticeable are the minima at $q \approx q_p$ and $q \approx 3$ Å$^{-1}$, with the latter related to the shoulder in $S(q)$. These features are also visible in the calculated OF-AIMD results for $T=373$ K, which show a fair agreement with experiment.

The transverse current correlation function $J_t(q,t)$ provides information on the shear modes and its shape evolves from a Gaussian, in both $q$ and $t$, at the free particle ($q \to \infty$) limit toward a Gaussian in $q$ and exponential in $t$ at the hydrodynamic limit ($q \to 0$), i.e.,

$$J_t(q \to 0,t) = \frac{1}{\beta m} e^{-q^2 \eta |t|/m\rho}, \tag{8}$$

where $\eta$ is the shear viscosity coefficient, $\beta=(k_B T)^{-1}$, and $m$ is the atomic mass. At both the above limits, $J_t(q,t)$ is always positive. However, at intermediate $q$ values, it usually shows a more complicated behavior with well-defined oscillations around zero,[17,18,36] whereas the associated spectra $J_t(q,\omega)$ have an inelastic peak which appears at low $q$ values and lasts for a finite $q$ range. Indeed, l-Ga at $T=373$ K clearly shows the aforementioned behavior which qualitatively agrees with what has already been obtained for other simple liquid metals[17,18,34] near melting. The associated spectra show clear inelastic peaks within the range of $0.3 \leq q \leq 2.30$ Å$^{-1}$. However, when the temperature is increased to $T=523$ K, the oscillations in $J_t(q,t)$ become weaker and now the inelastic peaks are confined to a narrower range; namely, $0.5 \leq q \leq 1.80$ Å$^{-1}$. At $T=959$ K, $J_t(q,t)$ show extremely weak oscillations and now the corresponding $J_t(q,\omega)$ has no inelastic peaks. This progressive disappearance of the inelastic peaks with increasing temperature can be observed in Fig. 4 where we have depicted $J_t(q,\omega)$ for $T=373$ and 959 K and a wide $q$ range. Recalling that the inelastic peaks in $J_t(q,\omega)$ are associated with propagating shear waves, the previous results point to its absence for l-Ga at $T=959$ K.

From the obtained $J_t(q,t)$, it is possible to estimate the shear viscosity coefficient $\eta$. The procedure exploits the

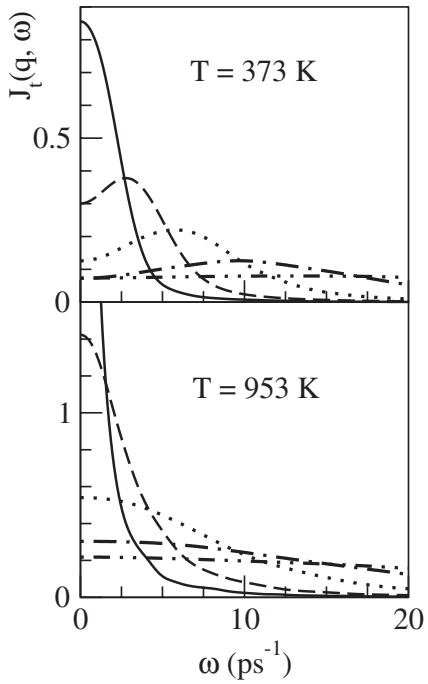


FIG. 4. OF-AIMF transverse current correlation spectrum $J_t(q,\omega)$ at several $q$ values (in Å$^{-1}$) for liquid Ga at $T=373$ and 953 K. $q=0.26$ (full curve), $q=0.45$ (dashed curve), $q=0.82$ (dotted curve), $q=1.3$ (dashed-dotted curve), and $q=1.9$ (dashed-double dotted curve).

memory function representation of the $J_t(q,t)$. Further details are given in Refs. 18, 37, and 38. From the present OF-AIMD simulations, we obtain the values (in GPa ps units) $\eta=1.60 \pm 0.20$ (for $T=373$ K), $\eta=1.12 \pm 0.15$ (for $T=523$ K), and $\eta=0.74 \pm 0.08$ (for $T=959$ K), which stand in reasonable agreement with their respective experimental data;[39] namely, $\eta_{\text{expt}}=1.58 \pm 0.05$, $\eta_{\text{expt}}=1.10 \pm 0.05$, and $\eta_{\text{expt}}=0.63 \pm 0.03$.

### 2. Single-particle dynamics

Information on the transport properties in liquid systems can be extracted from the velocity autocorrelation function (VACF) of a tagged ion in the fluid $Z(t)$ defined as

$$Z(t) = \langle \mathbf{v}_1(t)\mathbf{v}_1(0)\rangle / \langle v_1^2 \rangle, \tag{9}$$

which stands for the normalized VACF. Figure 5 shows the obtained $Z(t)$, which exhibit the usual pattern displayed by simple liquid metals; namely (i) an oscillatory behavior with a distinct negative minimum followed by progressively weaker oscillations and (ii) dampened features with increasing temperature (i.e., decreasing density).

The associated power spectrum $Z(\omega)$ is the time Fourier transform (FT) of $Z(t)$, and the results obtained are depicted in Fig. 6. At $T=373$ K, $Z(\omega)$ shows the double peak structure characteristic of simple liquid metals near melting,[17,18] However, as the temperature is increased the low frequency peak progressively fades away, whereas the low frequency diffusive modes become more conspicuous. Simultaneously, the higher frequency peak dampens and slightly moves to-

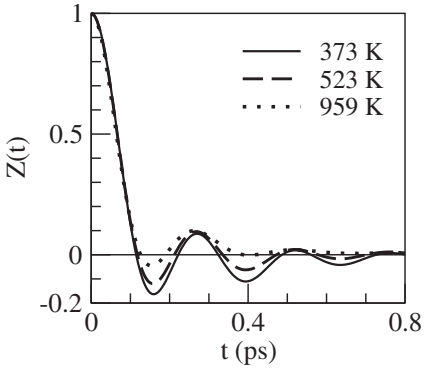


FIG. 5. Normalized OF-AIMD $Z(t)$ for l-Ga at three temperatures along the coexistence line.

ward smaller $\omega$ values. This is precisely the trend observed in Fig. 6 where we stress that at $T=959$ K the low frequency peak has already disappeared.

The self-diffusion coefficient $D$ is readily obtained from either the time integral of $Z(t)$ or from the slope of the mean square displacement $\delta R^2(t) \equiv \langle |\mathbf{R}_1(t) - \mathbf{R}_1(0)|^2 \rangle$ of a tagged ion in the fluid as follows:

$$D = \frac{1}{\beta m} \int_0^\infty Z(t)dt, \quad D = \lim_{t\to\infty} \delta R^2(t)/6t. \tag{10}$$

Both routes lead to practically identical values; namely, $D_{\text{OF-AIMD}}=0.20\pm0.02$, $0.38\pm0.02$, and $0.95\pm0.04$ Å$^2$/ps for $T=373$, 523, and 959 K, respectively. The experimental data[40] for l-Ga at melting ($T=303$ K) stand within the range of $D_{\text{expt}}\approx 0.16-0.17$ Å$^2$/ps, and extrapolation to $T=373$ K gives an estimate of $D_{\text{expt}}\approx 0.24-0.27$ Å$^2$/ps. As for the higher temperatures, no experimental data are available but we may compare with other calculations. For example, the KS-AIMD calculation at $T=1000$ K by Gong *et al.*[7] gave $D_{\text{KS-AIMD}}=1.0$ Å$^2$/ps, which is very close to the present OF-AIMD result. On the other hand, the KS-AIMD study of Holender *et al.*[8] at $T=982$ K yielded the much smaller value of $D_{\text{KS-AIMD}}=0.65$ Å$^2$/ps. All in all, the present OF-AIMD result stands within the range of values predicted by the KS-AIMD method.

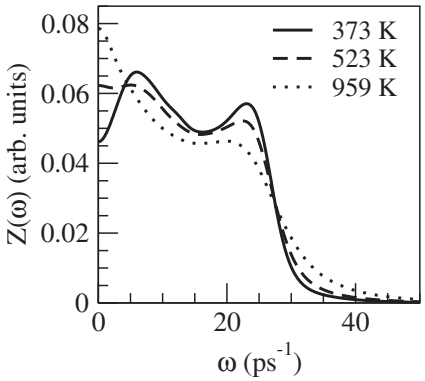


FIG. 6. Same as in the previous figure but for the corresponding power spectrum $Z(\omega)$.

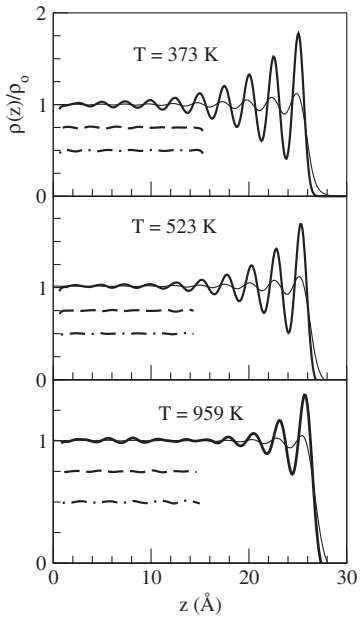


FIG. 7. Electronic (continuous thin line) and ionic (continuous thick line) density profiles normal to the liquid-vapor interface in liquid Ga at $T=373$, 523, and 959 K. The densities are plotted relative to their values at the slab's center. The dashed and dotted-dashed lines are the $x$-transverse (displaced by $-0.25$) and $y$-transverse (displaced by $-0.5$) ionic density profiles.

## IV. RESULTS: LIQUID-VAPOR INTERFACE

Additional OF-AIMD simulations have been performed in order to study the LV interfaces in l-Ga at $T=373$, 523, and 959 K. Now, for each system, we have considered a slab consisting of 3000 ions in a supercell with two free surfaces normal to the $z$ axis. The dimensions of the slabs were $L_0L_0L_z$ ($L_z=\alpha L_0$), with $\alpha=1.75$ and $L_0$ chosen so that the average ionic number density of the slab coincides with the experimental bulk ionic number density of the system at the same temperature; an additional 20 Å of vacuum was added both above and below the slab. The ionic time step was again $\delta t=0.005$ ps, but now we took $E_{\text{cut}}=10.5$ Ry for all systems. We used a smaller $E_{\text{cut}}$ than in the bulk calculations because the increased simulation box and number of ions imposed heavier computational demands. Nevertheless, we checked that even for this smaller cutoff, the energy and forces were well converged. An equilibration run of 15 ps was performed and the evaluation of the slab's physical properties was made by averaging over the following 90 ps.

During the simulations, the slabs slightly contracted in response to the zero external pressure condition, leading to some increase in the average ionic density in the central region of the slab with respect to its input value (see Table I). Specifically, those variations were 6.7% (at $T=373$ K), 7.6% (at $T=523$ K), and 9.5% (at $T=959$ K).

The longitudinal ionic DP was computed from a histogram of particle positions relative to the slab's center of mass, with the profiles from both halves of the slab being averaged; the results are shown in Fig. 7. There is a marked stratification lasting for several layers (ranging from $\approx 6-7$ for $T=373$ K to $\approx 3-4$ for $T=959$ K) with the outer oscil-

TABLE II. Details of the layers used for computing the transverse pair correlation functions $\Delta z_{OL}$ and $\Delta z_{SL}$ refer to the positions, with respect to the center of mass, of the outermost and second layers, respectively. $\Delta\rho_{OL}$ and $\Delta\rho_{SL}$ are the percent variations, with respect to the slab's bulk value, of the ionic number densities in the outermost and second layers, respectively.

| $T$ (K) | $\Delta z_{OL}$ (Å) | $\Delta z_{SL}$ (Å) | $\Delta\rho_{OL}$ | $\Delta\rho_{SL}$ |
|---|---|---|---|---|
| 373 | 23.8–25.9 | 21.3–23.8 | 18.4 | 0 |
| 523 | 24.07–26.27 | 21.54–24.07 | 12.0 | 0 |
| 959 | 24.4–26.75 | 21.8–24.4 | 5.1 | −2.7 |

lation displaying the higher amplitude. For each thermodynamic state, all of the oscillations have the same wavelength; namely, $\lambda=2.5$, 2.53, and 2.6 Å for $T=373$, 523, and 959 K, respectively. We note that these $\lambda$ values neatly fit into the linear relationship[41] that for several simple liquid metals, we have found between $\lambda$ of the oscillations in the longitudinal ionic DP and the radii of the associated Wigner–Seitz spheres. The outer layer, comprising from the outer minimum to that point of the decaying tail where it reaches half of its bulk value, has a smaller wavelength; namely, $\lambda=2.1$, 2.2, and 2.35 Å for $T=373$, 523, and 959 K, respectively. These features qualitatively agree with the "experimental" DP as derived from the XR measurements;[19–22] specifically, the experimental DP near melting exhibits oscillations with a $\lambda\approx2.55$ Å$^{-1}$ and the outer oscillation has a greater amplitude than the second one. Similar characteristics were also predicted by the MC simulations of Zhao *et al.*[23] for l-Ga at $T=373$ K; specifically, they also obtained an oscillating longitudinal ionic DP with $\lambda\approx2.5$ Å and the outer oscillation was again higher than the previous one. Figure 7 also includes the calculated transverse ionic DPs ($x$ and $y$), which are rather structureless in sharp contrast with the rich structure of the longitudinal ionic DP.

We have also analyzed the effects of the LV stratification on the in-plane structure of the liquid, as evidenced by the variation in the transverse pair correlation function $g_T(r)$ across the interface (Table II). We have partitioned the outer region of the slab into layers located between consecutive minima of the oscillations, with the narrower outer layer ranging as previously defined. The ionic number density of this outer layer and of the first inner one changes as shown in Table II, and all the inner layers have basically the bulk

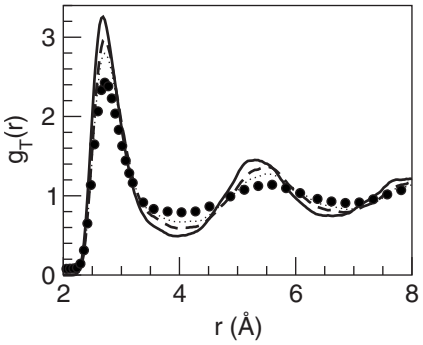


FIG. 8. Transverse pair correlation functions for the outer layers in l-Ga at $T=373$ K. Full line: outermost layer. Dashed line: first inner layer. Dotted line: second inner layer. Full circles: bulk $g(r)$.

value. Therefore, we observe that despite its marked stratification, the bulk density is attained at ≈6–7 Å from the LV interface. These density variations are reflected in the associated $g_T(r)$, whose main peak increases in height while preserving its position. This is depicted in Fig. 8 which shows $g_T(r)$ for the outer layers along with the bulk one. Those $g_T(r)$ have been used to calculate the CN within each layer, defined as the average number of neighbors within a distance identified as the position of the first minimum of the two-dimensional (2D) radial distribution function [which for these 2D layers is proportional to $rg_T(r)$].[42] The values obtained are CN=5.1, 5.0, and 4.9 for the outer, first, and second inner layers, respectively, whereas a similar calculation for a layer placed at the center of the slab yielded CN=4.7. The greater values at the outer layers are a consequence of the greater ionic number density and/or a higher main peak.

Additional insight into the three-dimesional local structure is provided by the $z$-dependent CN $n(z)$ defined as the average number of neighbors (notwithstanding its position) within a distance $r_m$ which is taken as the position of the first minimum of the bulk RDF (the specific values are given in the previous section). Table III gives the $n(z)$ values for selected locations inside the slab. Within a wide region around the center of the slab, $n(z)$ remains practically a constant and it is just very close to the LV interface; namely, around the second outer maximum when $n(z)$ begins to decrease. Indeed, even at this second outer maximum, $n(z)$ still takes the bulk value, whereas at the outer maximum, the $n(z)$ values have already decreased to ≈70%.

Another informative property concerns the structural rearrangements induced by the interface. Those changes may be

TABLE III. Values of the $z$-dependent coordination number $n(z)$ at different $z$ values along the slab. $n(z_B)$ is the average value in a wide region around the center of the slab. $z_{OM}$ and $z_{SM}$ are the positions of the outer maximum and the second maximum, respectively. $z_d$ is the distance between the outer maximum and the point where the decaying ionic density profile reaches half the bulk value. $n(z_d)$ is defined in the text.

| $T$ (K) | $n(z_B)$ | $z_{OM}$ (Å) | $n(z_{OM})$ | $z_{SM}$ (Å) | $n(z_{SM})$ | $z_d$ (Å) | $n(z_d)$ |
|---|---|---|---|---|---|---|---|
| 373 | 11.5 | 25.0 | 8.2 | 22.5 | 11.6 | 0.90 | 7.3 |
| 523 | 10.9 | 25.3 | 7.8 | 22.77 | 10.9 | 0.92 | 6.9 |
| 959 | 8.5 | 25.7 | 6.1 | 23.1 | 8.5 | 0.95 | 5.6 |

quantified[43] by comparison with an ideally terminated surface obtained by abruptly cutting the slab in the central region, i.e., at $z=0$. Then, $n(z)$ is evaluated at a distance $z_d$ which is approximately that between the outermost maximum and the point where the decaying ionic DP attains half its bulk value. The calculated values of $z_d$ and $n(z_d)$ are given in Table III. The $n(z_d)$ are always smaller than those at the outer maximum, which indicates that the surface structural rearrangements induce some increase in the CN over that of an ideally terminated surface.

Figure 7 also shows the calculated self-consistent valence electronic DP, which exhibits distinct oscillations although with much smaller amplitudes than those of the associated longitudinal ionic DP. The electronic oscillations are nearly in phase with those of the ionic DP. This feature is in sharp contrast with the MC results of Zhao *et al.*[23] for l-Ga at $T=373$ K, where their longitudinal ionic and valence electronic DPs clearly stood in a nearly perfect opposite phase. This feature was then rationalized in terms of a competition between the valence electronic kinetic energy contribution, which takes smaller values by a damping of the oscillations, and the interaction term between electrons and ions (mainly its Coulombic part). However, this explanation has recently been questioned and, based on *ab initio* results for several liquid metals, a different cause has been proposed.[41] Specifically it hinges on the interplay between the width ($\sigma$) of the pseudoatomic valence density and the separation of layers ($\lambda$) in the ionic DP. Indeed, three broad groups were identified: (i) those with a ratio of $0.62 \leq \sigma/\lambda \leq 0.64$, where the ionic and electronic DPs oscillated in the opposite phase (i.e., the alkalis), (ii) those with $0.44 \leq \sigma/\lambda \leq 0.47$ had ionic and electronic DPs nearly in phase (i.e., Tl and Si), and (iii) those with $0.55 \leq \sigma/\lambda \leq 0.59$ which showed an intermediate behavior (i.e., Mg, Ba, and Al). Now, for the l-Ga states considered here, we obtain $\sigma/\lambda=0.462$, 0.456, and 0.444 for $T=373$, 523, and 959 K, which unequivocally allocates them within the group where the ionic and electronic DPs stand nearly in phase.

From the previous longitudinal ionic DP, we have constructed the corresponding longitudinal total electronic DP; namely, $\rho_e^T(z)$. It was made by adding the self-consistent OF-AIMD valence electronic density profile and the total core electronic density profile. This latter one was calculated by superposing the core electronic density at the ionic sites, which had previously been derived by the KS-DFT-type calculation made to obtain the associated ionic local pseudopotential.[18] Since the core densities are rather narrow, their superposition gives a profile in phase with the ionic DP. Moreover, as Ga has 28 core and 3 valence electrons, the addition of the core and valence electronic densities leads to a total electronic DP whose phase practically coincides with that of the ionic DP, as can be observed in Fig. 9.

The experimental analysis of the LV interface is usually performed by XR and/or grazing incidence x-ray diffraction techniques which, in fact, probe the total electronic density distribution. In the XR technique, x-rays of wavelength $\lambda$ incident upon the liquid surface at an angle $\alpha$ are scattered at the same angle within the reflection plane defined by the incident beam and the surface normal. The reflected intensity

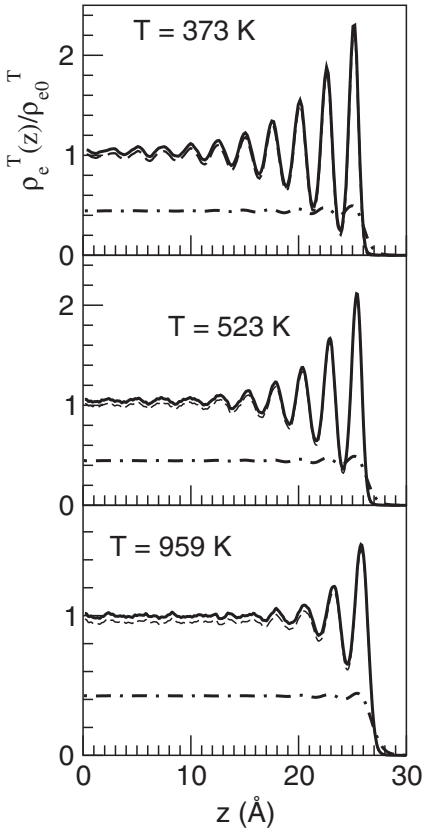


FIG. 9. Total electronic density profile (core plus valence) normalized to the slab's bulk value (thick continuous line). The dotted-dashed and dashed lines correspond to the valence (multiplied by a factor of ten) and core total electronic density profiles, respectively.

$R(q_z)$ is directly related[19–21] to the *intrinsic* (i.e., in the absence of capillary wave smearing) surface-normal (longitudinal) total (core plus valence) electronic density profile $\rho_{e,\mathrm{int}}^T(z)$,

$$R(q_z)/R_F(q_z) = |\Phi_{\mathrm{int}}(q_z)|^2 \exp(-\sigma_c^2 q_z^2), \tag{11}$$

where $q_z=(4\pi/\lambda)\sin\alpha$ is the momentum transfer perpendicular to the interface, $R_F(q_z)$ is the Fresnel reflectivity of a perfectly sharp step-function interface, and $\Phi_{\mathrm{int}}(q_z)$ is the intrinsic surface structure factor defined as

$$\Phi_{\mathrm{int}}(q_z) = \frac{1}{\rho_{e0}^T}\int_{-\infty}^{\infty}\left(\frac{\partial \rho_{e,\mathrm{int}}^T(z)}{\partial z}\right)\exp(iq_z z)dz, \tag{12}$$

where $\rho_{e0}^T$ is the bulk total electron density. The term $\exp(-\sigma_c^2 q_z^2)$ in Eq. (11) purports to account for the effects on $R(q_z)$ of the thermally excited capillary waves, with $\sigma_c$ being interpreted as an effective capillary wave roughness. We also recall that Eq. (11) holds for $q_z$ larger than about four times the critical wave vector $q_c$ for total external reflection ($q_c \approx 0.0483$ Å$^{-1}$ for l-Ga).

The total electron density profile that we obtain within the OF-AIMD simulations is, however, not the intrinsic profile because it includes some thermal fluctuations of the surface, as dictated by the temperature and the dimensions of the simulation box. Therefore, in order to compare our results

with the experimental ones, we have to take these effects into account. We will follow a kind of analysis similar to that taken up by the experimental group. They measured the reflectivity at several temperatures in the range from 295 to 443 K and analyzed the results in terms of the "distorted crystalline model," supplemented by a damping term that accounts for surface roughness. This leads to a convolution of the assumed intrinsic profile with a Gaussian function $\exp[-z^2/(2\sigma_c^2)]$ [which upon FT leads to the exponential term in Eq. (11)]. After the corresponding fit to the measured data, they found that $\sigma_c^2$ varies linearly with temperature, but takes a nonzero value in the limit $T=0$ K. Therefore, they proposed that two terms contribute to $\sigma_c^2$, an intrinsic term, $\sigma_0^2$, which is independent of the temperature, and another term that varies linearly with $T$, $\sigma_{\mathrm{cw}}^2$, so that

$$\sigma_c^2 = \sigma_0^2 + \sigma_{\mathrm{cw}}^2. \tag{13}$$

In particular, the value for $\sigma_0$ obtained from the fits is 0.37 Å. While the origin of this first (intrinsic) term is not clear, the second term is easy to rationalize in terms of thermally excited capillary waves, taking on the expression

$$\sigma_{\mathrm{cw}}^2 = \frac{k_B T}{2\pi\gamma} \ln\left(\frac{q_{\max}}{q_{\min}}\right), \tag{14}$$

where $k_B$ is Boltzmann's constant and $\gamma$ is the surface tension. The short and long wave vector cutoffs, $q_{\max}$ and $q_{\min}$, are determined by the ionic diameter and the instrumental resolution, respectively. Specifically, the values used in the analysis of the experimental data[20] were $q_{\max}=\pi/d \equiv 1.26$ Å$^{-1}$ ($d$ is the ionic diameter) and $q_{\min}=0.0064$ Å$^{-1}$.

Coming back to the analysis of the OF-AIMD results, we note that a possible measure of the surface roughness is given by the width of the last layer in the total electronic density profile $\rho_e^T(z)$. In fact, this is exactly $\sigma_c^2$ in the distorted crystalline model. Several ways to quantify this width are available (half-width at half height, standard deviation, etc.) out of which we have selected the standard deviation, although different procedures only slightly change the final value (for instance, at 373 K, the widths are 0.50 Å in the case of using the half-width at half height and 0.48 Å for the standard deviation). We have then calculated these widths of the last layer of $\rho_e^T(z)$ for $T=373$ and 523 K, and extrapolated the results to zero temperature in order to obtain the intrinsic contribution to surface roughness, $\sigma_0^{\mathrm{OF}}=0.44$ Å, a value somewhat larger than the experimental one. The capillary wave term in the surface roughness has to be considered carefully in order to make a meaningful comparison between the reflectivity curves obtained from simulation and experiment. The reason is that while the value of $q_{\min}^{\mathrm{expt}}$ in Eq. (14) is dictated by instrumental resolution in the experimental case, in the simulations it is dictated by the transverse area ($L^2$) of the simulation box, $q_{\min}^{\mathrm{OF}}=\pi/L$, and this value is far greater than the experimental one. Therefore, the value of the capillary wave contribution to surface roughness $\sigma_{\mathrm{cw}}$ is smaller in the simulation than in the experiment ($\sigma_{\mathrm{cw}}^{\mathrm{OF}} < \sigma_{\mathrm{cw}}^{\mathrm{expt}}$) and we have to take this difference into account in the comparison.

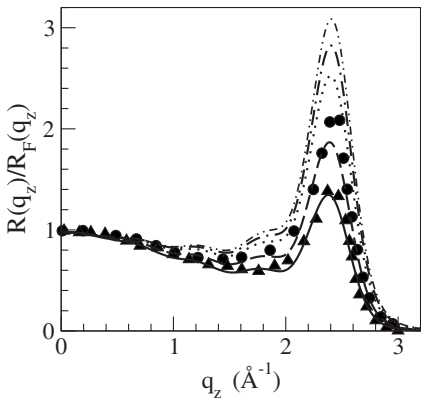


FIG. 10. Fresnel normalized reflectivity curves of liquid Ga. Full circles and triangles: Experimental results (Refs. 19 and 20) at $T=360$ and 397 K, respectively. Continuous, dashed, dotted, dotted-dashed, and double dotted-dashed lines: OF-AIMD results for $T=373$ K using intrinsic surface roughness $\sigma_0^{\mathrm{OF}}=0.60$, 0.55, 0.50, 0.48, and 0.44 Å, respectively.

In practice, this translates into the following procedure: first the total electron density profile $\rho_e^T(z)$ is obtained from the OF-AIMD simulation, then the surface structure factor,

$$\Phi(q_z) = \frac{1}{\rho_{e0}^T} \int_{-\infty}^{\infty} \left(\frac{\partial \rho_e^T(z)}{\partial z}\right) \exp(iq_z z) dz, \tag{15}$$

is computed. Its squared module already contains the capillary waves implicit in the simulation, so the final reflectivity is computed as

$$\frac{R(q_z)}{R_F(q_z)} = |\Phi(q_z)|^2 \exp[-((\sigma_0^{\mathrm{OF}})^2 + \Delta\sigma_{\mathrm{cw}}^2) q_z^2], \tag{16}$$

where $\Delta\sigma_{\mathrm{cw}}^2=(\sigma_{\mathrm{cw}}^{\mathrm{expt}})^2-(\sigma_{\mathrm{cw}}^{\mathrm{OF}})^2$, i.e., from the total capillary damping, we substract that already present in the simulation.

Figure 10 shows the calculated OF-AIMD results for $R(q_z)/R_F(q_z)$ at $T=373$ K, obtained using[40] $\gamma=0.710$ N/m, along with the experimental data at 360 and 397 K. There is qualitative agreement with experiment and the peak's position is correctly given although its height is overestimated. Nevertheless, we emphasize the extreme sensitivity of the calculated $R(q_z)/R_F(q_z)$ to the values used for the intrinsic contribution; specifically, we have again calculated the OF-AIMD results for $R(q_z)/R_F(q_z)$ with $\sigma_0^{\mathrm{OF}}=0.48$, 0.50, 0.55, and 0.60 Å. Now, as shown in Fig. 10, the results obtained show a better agreement with experiment along the whole $q_z$ range, with the position and magnitude of both the minimum and the peak being reasonably reproduced.

The origin of the intrinsic contribution is not yet clear although it has been related to the finite atomic size; however, its role seems essential in order to properly describe the experimental $R(q_z)/R_F(q_z)$ curves. In the present OF-AIMD calculations at $T=373$ K, the contribution of the $\sigma_0^2$ term to the total value of $\sigma_c^2$ [see Eq. (13)] was ≈24%, whereas in the distorted crystalline model used to fit the experimental data,[19,20] the corresponding contribution of the $\sigma_0^2$ term was somewhat smaller, ≈18%.

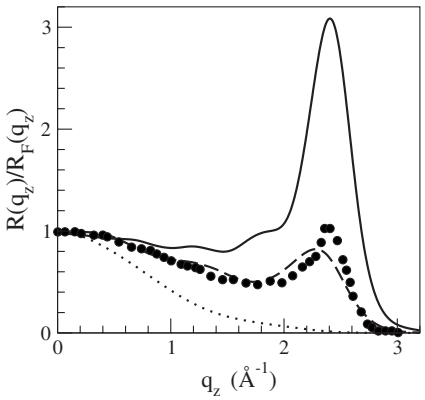


FIG. 11. Fresnel normalized reflectivity curves of liquid Ga. Full circles: experimental results (Ref. 20) at $T=443$ K. Continuous, dashed, and dotted lines: calculated OF-AIMD results for $T=373$, 523, and 959 K, respectively.

The calculated OF-AIMD results for the $R(q_z)/R_F(q_z)$ at $T=523$ and 959 K are depicted in Fig. 11. As already mentioned, we took $\sigma_0=0.44$ Å, whereas the $\sigma_{\mathrm{cw}}^{\mathrm{expt}}$ term was calculated by using the same $q_{\max}$ and $q_{\min}^{\mathrm{expt}}$ as in the experimental setup, while the corresponding $q_{\min}^{\mathrm{OF}}$ was obtained from the simulation box. For the surface tension, we have taken the experimental values[40] $\gamma=0.700$ and 0.675 N/m for $T=523$ and 959 K, respectively. Table IV shows the values used for both $\sigma_0$, $\sigma_{\mathrm{cw}}^{\mathrm{expt}}$, and $\sigma_{\mathrm{cw}}^{\mathrm{OF}}$ at the three thermodynamic states. According to Fig. 11, when the temperature increases, the peak's height is substantially reduced, and at $T=959$ K, the peak has already vanished. Indeed, the experimental $R(q_z)/R_F(q_z)$ curves for the range of 293–433 K have shown that as the temperature was increased the peak's height quickly reduced although its width remained practically unchanged. This dampening of the peak's height comes as a consequence of the capillary waves, which become stronger with increasing temperature.

As evidenced in Fig. 11, the OF-AIMD calculations for $T=523$ K give a value of $\approx 0.80$ for the peak's height, which is fairly close to the value of $\approx 0.70 \pm 0.05$ derived from an extrapolation of the experimental data. Finally, concerning the peak's width, we have calculated the variance of the curves associated with the peaks at $T=373$ and 523 K and we obtained the values of 0.22 and 0.24, respectively. This small variation is in partial agreement with the experimental observation, based on the temperature range of 293–433 K, where the peak's width remained practically unchanged with increasing temperature.

TABLE IV. Values (in Å) of the effective capillary roughness $\sigma_c$ and its two contributions $\sigma_0$ and $\sigma_{\mathrm{cw}}^{\mathrm{expt}}$. We have also included the simulation capillary wave roughness $\sigma_{\mathrm{cw}}^{\mathrm{OF}}$.

| $T$ (K) | $\sigma_c$ | $\sigma_0$ | $\sigma_{\mathrm{cw}}^{\mathrm{expt}}$ | $\sigma_{\mathrm{cw}}^{\mathrm{OF}}$ |
|---|---|---|---|---|
| 373 | 0.896 | 0.44 | 0.78 | 0.52 |
| 523 | 1.03 | 0.44 | 0.93 | 0.63 |
| 959 | 1.35 | 0.44 | 1.28 | 0.88 |

## V. CONCLUSIONS

We have reported results of MD simulations for several bulk properties as well as the liquid-vapor interface of l-Ga at three thermodynamic states along the coexistence curve. The simulations have been performed using the orbital-free *ab initio* molecular dynamics method combined with a first-principles local pseudopotential constructed within the same framework. The method calculates the electronic structure and its influence on the forces among the ions at each step of the dynamics. Therefore, the substantial variations in electron density associated with the liquid-vapor interface are accounted for in the forces, allowing a reliable study of the interfaces.

Concerning bulk l-Ga, the results obtained for the static structure are comparable to those obtained by previous KS-AIMD calculations[7,8] and, more importantly, they are in reasonable agreement with the available experimental data.[9,10] A similar level of agreement with experiment is also achieved for the dynamic properties which, on the other hand, show the typical features of simple liquid metals, such as (i) an oscillatory behavior of the intermediate scattering functions at low-$q$ values, (ii) collective density excitations in the dynamic structure factors up to $q \approx (3/5)q_p$, and (iii) shear modes in the transverse current correlation function.

Additional simulations were also performed for the liquid-vapor interface of l-Ga at those thermodynamic states. The calculations used slabs wide enough so as to rule out possible interference effects between the two free surfaces, and are placed in supercells which are large enough to disregard slab-slab interactions.

The calculated ionic density profiles show marked oscillations lasting for several layers, although with increasing temperature both the range and amplitude of the oscillations are reduced. The relative amplitudes as well as the wavelengths of the oscillations agree with the experimental data. The self-consistent valence electronic density profiles also exhibit clear oscillations, which are practically in phase with the ionic ones. This is in contrast with previous studies, and we provide a rationale based on the interplay between the width of the atomic valence density and that of the ionic layers. Parenthetically, this explanation has also accounted for the variety of relative phases between the ionic and valence electronic density profiles obtained for the LV interface in a wide range of simple liquid metals.[41]

From the previous density profiles, we have evaluated the total electronic density profile (which is the physical magnitude probed in the x-ray reflectivity measurements) and therefrom the associated reflected intensity $R(q_z)$. This latter step involves accounting for the surface roughness $\sigma_c$, which appears in the form of a Debye-Waller-type factor [see Eq. (11)]. $\sigma_c$ has two contributions, including the capillary wave term and an intrinsic one $\sigma_0$, whose origin is not yet clear. Given its interpretation as a measure of the width of the outer layer in the intrinsic total electronic density profile $\rho_{e,\mathrm{int}}^{T}(z)$, we have estimated it as an extrapolation from the OF-AIMD results at $T=373$ and 523 K to 0 K.

On the other hand, improvements can also be made in the calculation of $\sigma_{\mathrm{cw}}$. Specifically, the present study has used the experimental value for the surface tension $\gamma$ in Eq. (14),

but a more consistent approach would require one to include a value calculated within the same OF-AIMD scheme. Indeed, this is not a minor point; for instance, at $T=373$ K, a reduction of $\gamma$ by a mere 15% results in a decrease in the reflectivity peak's height by 30%.

In any case, we stress the remarkable sensitivity of the calculated $R(q_z)/R_F(q_z)$ curves to the value of the $\sigma_c$ in Eq. (11). However, at the very least, the calculated OF-AIMD curves plotted in Fig. 10 show that by choosing an appropriate value for $\sigma_c$, it is possible to achieve a very good description of the whole experimental curve over the whole $q_z$ range. Therefore, it appears that further improvements may come from a more thorough investigation into the contributions to $\sigma_c$.

## ACKNOWLEDGMENTS

We acknowledge the financial support of the DGICYT of Spain (MAT2005-03415), Junta de Castilla y León (VA068A06), and the EU FEDER program.

[1] P. Hohenberg and W. Kohn, Phys. Rev. **136**, B864 (1964); W. Kohn and L. J. Sham, *ibid.* **140**, A1133 (1965).
[2] J. E. Inglesfield, J. Phys. C **1**, 1337 (1968).
[3] X. G. Gong, G. L. Chiarotti, M. Parrinello, and E. Tosatti, Phys. Rev. B **43**, 14277 (1991).
[4] K. K. Mon, N. W. Ashcroft, and G. V. Chester, Phys. Rev. B **19**, 5103 (1979).
[5] J. L. Bretonnet and C. Regnaut, Phys. Rev. B **31**, 5071 (1985); M. Boulahbak, J.-F. Wax, N. Jakse, and J. L. Bretonet, J. Phys.: Condens. Matter **9**, 4017 (1997); S. K. Lai, K. Horii, and M. Iwamatsu, Phys. Rev. E **58**, 2227 (1998).
[6] J. Hafner and W. Jank, Phys. Rev. B **42**, 11530 (1990).
[7] X. G. Gong, G. L. Chiarotti, M. Parrinello, and E. Tosatti, Europhys. Lett. **21**, 469 (1993).
[8] J. M. Holender, M. J. Gillan, M. C. Payne, and A. D. Simpson, Phys. Rev. B **52**, 967 (1995).
[9] M.-C. Bellissent-Funel, R. Bellissent, and G. Tourand, J. Phys. F: Met. Phys. **11**, 139 (1981); M.-C. Bellissent-Funel, P. Chieux, D. Levesque, and J. J. Weis, Phys. Rev. A **39**, 6310 (1989).
[10] Y. Waseda, *The Structure of Non-Crystalline Materials* (McGraw-Hill, New York, 1980).
[11] F. J. Bermejo, M. Garcia-Hernandez, J. L. Martinez, and B. Hennion, Phys. Rev. E **49**, 3133 (1994).
[12] F. J. Bermejo, R. Fernandez-Perea, M. Alvarez, B. Roessli, H. E. Fischer, and J. Bossy, Phys. Rev. E **56**, 3358 (1997).
[13] L. E. Bove, F. Formisano, F. Sacchetti, C. Petrillo, A. Ivanov, B. Dorner, and F. Barocchi, Phys. Rev. B **71**, 014207 (2005).
[14] T. Scopigno, A. Filipponi, M. Krisch, G. Monaco, G. Ruocco, and F. Sette, Phys. Rev. Lett. **89**, 255506 (2002).
[15] T. Scopigno, R. Di Leonardo, L. Comez, A. Q. R. Baron, D. Fioretto, and G. Ruocco, Phys. Rev. Lett. **94**, 155301 (2005).
[16] S. Hosokawa, W.-C. Pilgrim, H. Sinn, and E. E. Alp, Physica B (Amsterdam) **350**, 262 (2004).
[17] U. Balucani and M. Zoppi, *Dynamics of the Liquid State* (Clarendon, Oxford, 1994); J. P. Hansen and I. R. McDonald, *Theory of Simple Liquids* (Academic, London, 1986).
[18] D. J. González, L. E. González, J. M. López, and M. J. Stott, Phys. Rev. B **65**, 184201 (2002).
[19] M. J. Regan, E. H. Kawamoto, S. Lee, P. S. Pershan, N. Maskil, M. Deutsch, O. M. Magnussen, B. M. Ocko, and L. E. Berman, Phys. Rev. Lett. **75**, 2498 (1995).
[20] M. J. Regan, P. S. Pershan, O. M. Magnussen, B. M. Ocko, M. Deutsch, and L. E. Berman, Phys. Rev. B **54**, 9730 (1996).
[21] M. J. Regan, P. S. Pershan, O. M. Magnussen, B. M. Ocko, M. Deutsch, and L. E. Berman, Phys. Rev. B **55**, 15874 (1997).
[22] B. Lin, M. Meron, J. Gebhardt, T. Graber, D. Li, B. Yang, and S. A. Rice, Physica B (Amsterdam) **357**, 106 (2005).
[23] M. Zhao, D. S. Chekmarev, Z. H. Cai, and S. A. Rice, Phys. Rev. E **56**, 7033 (1997).
[24] M. Zhao, D. S. Chekmarev, and S. A. Rice, J. Chem. Phys. **109**, 1959 (1998).
[25] J. P. Perdew, K. Burke, and M. Ernzerhof, Phys. Rev. Lett. **77**, 3865 (1996); **78**, 1396 (1997).
[26] F. Perrot, J. Phys.: Condens. Matter **6**, 431 (1994); E. Smargiassi and P. A. Madden, Phys. Rev. B **49**, 5220 (1994); M. Foley and P. A. Madden, *ibid.* **53**, 10589 (1996).
[27] J. Blanco, D. J. González, L. E. González, J. M. López, and M. J. Stott, Phys. Rev. E **67**, 041204 (2003); D. J. González, L. E. González, J. M. López, and M. J. Stott, *ibid.* **69**, 031205 (2004).
[28] D. J. González, L. E. González, and M. J. Stott, Phys. Rev. Lett. **92**, 085501 (2004); **94**, 077801 (2005).
[29] M. Inui, S. Takeda, and T. Uechi, J. Phys. Soc. Jpn. **61**, 3203 (1992).
[30] N. E. Cusak, *The Physics of Structurally Disordered Matter* (Adam Hilger, Bristol, 1987).
[31] R. L. McGreevy, A. Baranyai, and I. Ruff, Phys. Chem. Liq. **16**, 47 (1986).
[32] A. Torcini, U. Balucani, P. H. K. de Jong, and P. Verkerk, Phys. Rev. E **51**, 3126 (1995).
[33] F. Shimojo, K. Hoshino, and M. Watabe, J. Phys. Soc. Jpn. **63**, 141 (1994).
[34] S. Kambayashi and G. Kahl, Phys. Rev. A **46**, 3255 (1992); G. Kahl and S. Kambayashi, J. Phys.: Condens. Matter **6**, 10897 (1994).
[35] J. Casas, D. J. González, and L. E. González, Phys. Rev. B **60**, 10094 (1999); J. Casas, D. J. González, L. E. González, M. M. G. Alemany, and L. J. Gallego, *ibid.* **62**, 12095 (2000).
[36] J. P. Boon and S. Yip, *Molecular Hydrodynamics* (Dover, New York, 1991).
[37] B. J. Palmer, Phys. Rev. E **49**, 359 (1994).
[38] U. Balucani, J. P. Brodholt, P. Jedlovszky, and R. Vallauri, Phys. Rev. E **62**, 2971 (2000).
[39] J. Vollmann and D. Riedel, J. Phys.: Condens. Matter **8**, 6175 (1996).
[40] T. Iida and R. I. L. Guthrie, *Physical Properties of Liquid Metals* (Clarendon, Oxford, 1988), p. 200.
[41] L. E. González, D. J. González, and M. J. Stott, J. Chem. Phys. **123**, 201101 (2005).
[42] D. J. González, L. E. González, and M. J. Stott, Phys. Rev. B **74**, 014207 (2006).
[43] G. Fabricius, E. Artacho, D. Sanchez-Portal, P. Ordejon, D. A. Drabold, and J. M. Soler, Phys. Rev. B **60**, R16283 (1999).